RSC Advances

ROYAL SOCIETY OF CHEMISTRY

www.rsc.org/advances

Journal Name

ARTICLE

Synthesis and study of hybrid hydrogen-bonded bent-core liquid crystal complexes containing C_{60}- and Si-based proton donors†

Received 00th January 20xx,
Accepted 00th January 20xx

DOI: 10.1039/x0xx00000x

www.rsc.org/

Shih-Hsien Liu,[a] Chong-Lun Wei,[a] I-Hung Chiang,[a] Chun-Yen Liao,[a] Chinmayananda Gouda,[a] Reguram Arumugaperumal,[a] Wei-Tsung Chuang,[b] Jey-Jau Lee,[b] Yu-Chie Chen[c] and Hong-Cheu Lin*[a]

Novel hydrogen-bonded (H-bonded) C_{60}- and Si-based bent-core liquid crystal (LC) complexes containing a bent-shaped proton acceptor and C_{60}- and Si-based single/double armed proton donors were synthesized and mingled to produce hybrid H-bonded LC complexes. The SmCP phases were able to be introduced in the hybrid LC complexes with a very high C_{60}-based moiety up to 90 mol%. Among our H-bonded LC complexes, the hybrid LC complexes with low contents of the C_{60}-based moiety (≦ 24 mol%) possessed the highest spontaneous polarization value (ca. 494 nC/cm^2), the widest mesophasic range (40.8°C) and the lowest saturated electric field (8.8 Vpp/μm). Under electric fields of modified triangle waveforms, both series of hybrid H-bonded LC complexes displayed an anti-ferroelectric (AF) to a ferroelectric (FE) polar switching as the C_{60}-based moiety increased up to 24-50 mol%. Therefore, the hybrid H-bonded LC complexes containing a broad molar ratio (0-90 mol%) of C_{60}-based moiety reveled a tunable route for the electro-optical applications of C_{60}-based H-bonded liquid crystals.

Introduction

Buckyball (also named as buckminsterfullerene or [60]fullerene) is a structure of truncated icosahedron with formula C_{60}, which was first synthesized by Kroto et al. in 1985.[1] The buckyball structure displays various special properties, such as observable wave-particle duality,[2] superconductivity,[3-6] non-linear optical property[7] and high electronic affinity.[8,9] Moreover, with proper surface modification, its derivatives showed extensive applications, e.g., hydration,[10-12] hydrogenation,[13,14] halogenation,[14] oxygenation,[15,16] cycloaddition,[17-19] free radical reaction,[20] photoreaction,[21,22] endohedral metallofullerene,[23,24] catalyst,[25] biomedical sensor/therapy[26,27] and electron acceptor.[28,29] The arrangements of charge transporting materials (e.g., buckyballs) were drawn much attention recently due to the improving of charge transfer in molecular electronics.[30-36] By attaching to mesogens, [60]fullerene could be aligned via liquid crystalline mesophases, and the methods were luxuriant (including some cost-effective ways) to enhance the arrangements of buckyballs.[31,37-50] With the advantages of easy-manipulating and flexible ratio-control (also reported as an effective conduit for charge transfer),[51] hydrogen-bonds (H-bonds) were our aim to be introduced to the C_{60}-based liquid crystal (LC) systems.[52] The electro-optical properties of fullerene-based LCs have been determined in the smectic[53] and columnar[49] phases accompanied with the molecular arrangements as well as the orientations of π-conjugated cores in mesophases to provide essential information for practical appearances.[54a-c] However, the electro-optical performance of C_{60}-based FLCs are rare,[54d] especially for those with H-bonds. Therefore, the combination of H-bonding, bent-core LCs, and fullerenes in this study are required for further investigations on their mesomorphic and electro-optical aspects. However, to our best knowledge, no hybrid H-bonded C_{60}-based liquid crystals have been synthesized up to date, which may be resulted from the weak H-bonding between proton donors and acceptors as well the strong aggregation of C_{60} nanoparticles (NPs) to disturb the arrangements of mesogens.[55] Therefore, an efficient blending method was applied to induce and stabilize the mesophases of H-bonded C_{60}-based LCs in our research. Moreover, LCs with ferro- and anti-ferroelectricities were utilized to reinforce the control of the applied electric fields as well as strengthen the photovoltaic effect on charge transporting materials.[56-60] According to the previous research of Ros et al.,[37] covalent-bonded bent-core LCs based on [60]fullerene displayed broad ranges of SmCP phase and novel physical properties. Hence, as shown in Figs. 1 and ,

[a] Department of Materials Science and Engineering, National Chiao Tung University, Hsinchu 30049, Taiwan. Fax: 8863-5724727; Tel: 8863-5712121 ext.55305. E-mail: linhc@mail.nctu.edu.tw.
[b] National Synchrotron Radiation Research Center, Hsinchu 30076, Taiwan.
[c] Department of Applied Chemistry, National Chiao Tung University, Hsinchu 30049, Taiwan.

† Electronic Supplementary Information (ESI) available: The details of synthetic steps and the elemental characterization of components **FIA**, **FIIA**, **IIA**, **SiA** and **NBF14**; the setup of P_s value measurement; the blending ratios of hybrid complexes; POM images of **FIA24** and **FIIA24**; crystallographic parameters of synthesized compounds and hybrid complexes; P_s values vs. applied electric fields of **FIAx** and **FIIAx**. See DOI: 10.1039/x0xx00000x

various H-bonded C_{60}-based bent-core complexes, i.e., **FIA100** and **FIIA100** (analogue **IIA100** without C_{60} as a comparison), were synthesized and investigated in this study, where a bent-shaped proton acceptor **NBF14** and the corresponding proton donors **FIA**, **FIIA** and **IIA** were prepared. In addition, the previously reported H-bonded Si-based bent-core complex **SiA100** containing the proton donor **SiA** was utilized as a LC host to mix with Au-based covalent-bonded bent-core dopant in order to facilitate the smectic alignment of Au-nanoparticles by electric fields.[61] Furthermore, the Si-based bent-core LC complex **SiA100** in this survey was also mingled with both H-bonded C_{60}-based bent-core complexes **FIA100** and **FIIA100** to induce and even extend the mesophasic ranges of the hybrid H-bonded bent-core LCs.

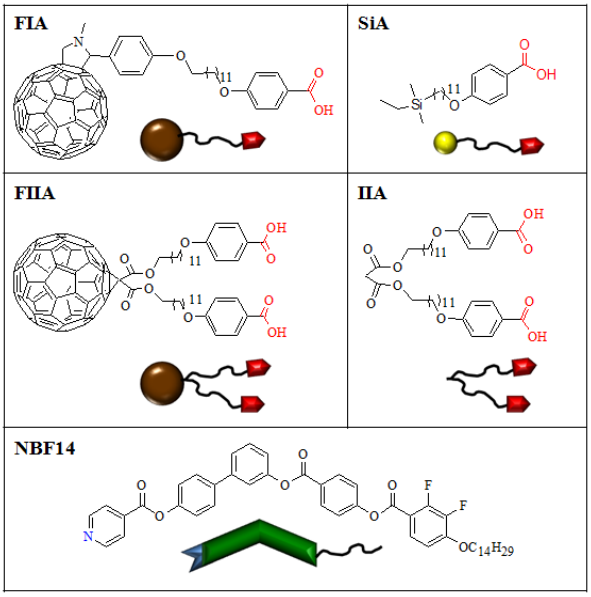

Fig. 1 Molecular structures of proton donors **FIA**, **FIIA**, **SiA** and **IIA** as well as a proton acceptor **NBF14**.

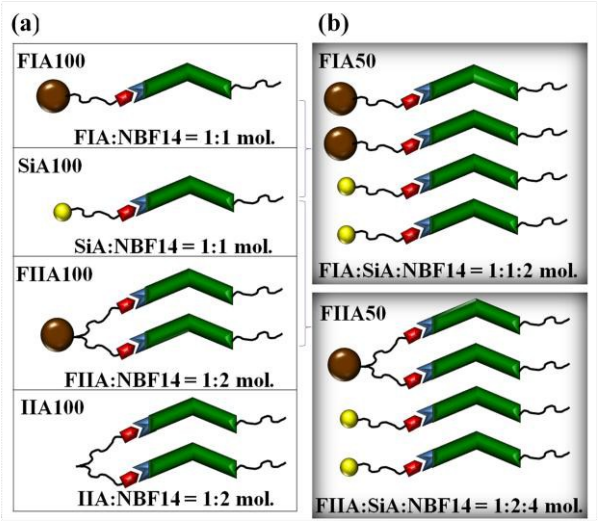

Fig. 2 (a) H-bonded bent-core complexes **FIA100**, **FIIA100**, **SiA100** and **IIA100**; (b) hybrid LC complexes **FIA50** and **FIIA50** containing 50% molar ratio of **SiA100** and 50% molar ratio of **FIA100** and **FIIA100**, respectively.

Notably, with a minor molar ratio of **SiA100** (i.e., 10 mole%), the hybrid H-bonded bent-core LC complexes containing both Si-based **SiA100** and C_{60}-based **FIA100** (or **FIIA100**) were able to display SmCP phases, and the electro-optical as well as mesophasic properties could be manipulated and optimized via the blending ratio of the Si- and C_{60}-based complexes, which could be more easily controlled than the covalent-bonded C_{60}-based LC systems.

Experimental

Synthesis. Synthetic steps of components **FIA**, **FIIA**, **IIA**, **SiA** and **NBF14** are shown in **Scheme S1** in the Supporting Information. Chemical characterization data of **FIA**, **FIIA**, **IIA**, **SiA** and **NBF14** are provided below:

4-((12-(4-(1-methylfulleropyrrolidin-2- yl)phenoxy)dodecyl)oxy) benzoic acid, (**FIA**). ^{1}H NMR (300 MHz, $CDCl_3$) δ (ppm): 8.00 (d, *J* = 9.0 Hz, 2H), 7.40 (m, 4H), 6.88 (d, 2H), 4.96 (d, *J* = 9.0 H 1H), 4.87 (s, 1H), 4.22 (d, *J* = 9.0 Hz, 1H), 4.01-3.92 (m, 4H), 2.78 (s, 3H), 1.75 (m, 4H), 1.36-1.23 (m, 16H). ^{13}C NMR (MHz, $CDCl_3$) δ (ppm) = 26.26, 29.38, 29.84, 30.60, 34.49, 40.29, 66.61, 68.23, 68.48, 70.22, 114.37, 114.81, 122.50, 124.73, 128.35, 128.95, 136.08, 139.83, 140.16, 140.41, 141.79, 141.94, 142.08, 142.25, 143.4, 144.65, 144.87, 144.97, 145.39, 145.52, 145.59, 145.76, 146.03, 146.38, 146.46, 146.55, 147.07, 147.33, 147.55, 159.44, 163.32, 166.49. Anal. Calcd for $C_{88}H_{39}NO_4$: C, 90.01; H, 3.35; N, 1.19. Found: C, 90.58; H, 2.86; N, 0.99. MS (FAB-) *m/z*: 1173.3 (exact mass); found, 1174.6.

4,4'-(((malonylbis(oxy))bis(dodecane-12,1-diyl))bis(oxy))(1,2-methanofullerene C_{60})-61,61-dibenzoic acid, (**FIIA**). ^{1}H NMR (300 MHz, $CDCl_3$) δ (ppm):7.96 (d, *J* = 9.0 Hz, 4H), 6.90 (d, *J* = 8.8 Hz, 4H), 4.47 (m, *J* = 6.6 Hz, 4H), 4.01 (t, *J* = 6.6 Hz, 4H 1.89 (m, 8H), 1.43–1.29 (m, 32H). ^{13}C NMR (75 MHz, $CDCl_3$) δ (ppm) = 26.01, 28.52, 29.13, 29.21, 29.40, 29.58, 67.31, 68.18, 114.05, 122.30, 131.55, 138.50, 138.59, 138.67, 139.12, 139.13, 139.18, 140.13, 140.34, 141.02, 141.20, 141.54, 141.84, 142.05, 142.32, 142.51, 142.85, 143.02, 143.36, 143.57, 144.01, 144.34, 144.58, 145.09, 145.11, 145.28, 145.37, 145.54, 146.02, 146.15, 146.45, 146.93, 147.21, 147.68, 162.93, 166.89. Anal. Calcd for $C_{101}H_{58}O_{10}$: C, 84.74; H, 4.08. Found: C, 85.33; H, 4.55. MS (FAB+) *m/z*: 1430.4 (exact mass); found, 1431.1.

4,4'-(((malonylbis(oxy))bis(dodecane-12,1-diyl))bis(oxy)) dibenzoic acid, (**IIA**). ^{1}H NMR (300 MHz, DMSO-d_6) δ (ppm) = 7.85 (d, *J* = 9.0 Hz, 4H), 6.97 (d, *J* = 8.7 Hz, 4H), 4.05–3.97 (m, 8H), 3.46 (s, 2H), 2.11–2.00 (m, 8H). 1.80–1.50 (m, 8H), 1.45–1.30 (m, 24H) Anal. Calcd for $C_{41}H_{60}O_{10}$: C, 69.07; H, 8.48. Found: C, 68.77; H, 8.41.

4-(Dimethylethylsiloxyl) undecyloxybenzoic acid, (**SiA**). The H-donor **SiA** was synthesized and reported in the reference,[61] NMR (300 MHz, CDC_{l3}) δ (ppm): 8.05 (d, *J* = 9.0 Hz, 2H), 6.95 (*J* = 9.0 Hz, 2H), 4.05 (t, *J* = 6.6 Hz, 2H), 1.81 (m, 2H),1.52–1.3 (m, 16H), 0.92 (t, *J* = 8.1 Hz, 3H), 0.48 (t, *J* = 7.8 Hz, 4H), 0.01 6H). Anal. Calcd for $C_{22}H_{38}O_3Si$: C, 69.79; H, 10.12. Found: C

69.62; H, 10.05. MS ($^+$) m/z: 378.26 (exact mass); found, 378 (M^+).

3'-(4-(2,3-Difluoro-4-(tetradecyloxy)benzoyloxy)benzoyloxy) biphenyl-4-yl isonicotinate, (**NBF14**). ^{1}H NMR (300 MHz, $CDCl_3$) δ (ppm): 8.87 (d, 2H), 8.29 (d, *J* = 8.3 Hz, 2H), 8.02 (d, *J* = 8.4 Hz, 2H), 7.86 (m, 1H), 7.67 (d, *J* = 8.2 Hz,2H), 7.54 (d, *J* = 4.7 Hz, 2H), 7.46 (s, 1H), 7.42 (d, *J* = 8.5 Hz, 2H), 7.31 (d, *J* = 8.7 Hz, 2H), 7.23−7.19 (m, 1H), 6.89−6.82 (m, 1H), 4.10 (t, *J* = 6.3 Hz, 2H), 1.80−1.75 (m, 2H), 1.43−1.28 (m, 22H), 0.86 (t, *J* = 6.3 Hz, 3H). Anal. Calcd for $C_{46}H_{47}F_2NO_7$: C, 72.33; H, 6.20; N, 1.83. Found: C, 72.15; H, 6.42; N, 1.83.

Sample preparation. The H-bonded complexes were prepared by dissolving proton acceptor **NBF14** and proton donors **FIA**, **FIIA**, **SiA** or **IIA** with equimolar amounts of pyridyl and benzoic acid groups in anhydrous tetrahydrofuran (THF). After each LC mixture was slowly evaporated at room temperature, the THF was completely removed in vacuum for 24 h, and then the hybrid LC complexes were obtained.

Characterization. ^{1}H and ^{13}C NMR spectra were verified with Varian Unity 300 MHz spectrometer. Mass spectra and elemental analyses were determined with Micromass TRIO-2000 GC-MS and Perkin-Elmer 240C elemental analyzer, respectively. MALDI-TOF measurements were carried out on AutoFlex III MALDI mass spectrometer (Bruker Daltonics, Breman, Germany). Fourier transform infrared spectra (FTIR) were recorded on a Perkin-Elmer Spectrum 100 Series with pressed KBr pellets. Mesophasic patterns, enthalpies of mesophase transitions and X-ray diffraction (XRD) were measured with polarizing optical microscope (POM, Leica DMLP; equipped with a hot stage, Linkam TMS-94/LTS350), differential scanning calorimeter (DSC, Perkin Elmer Diamond; rate 5°C/min of heating or cooling) and synchrotron X-ray radiation (at beamlines BL13A1, BL17A1 and BL01C2 at National Synchrotron Radiation Research Center, NSRRC, Taiwan), respectively. Typical X-ray scattering patterns were obtained with detectors (marCCD165 or mar345 image plates) for 1 to 30 seconds. The scattering angles were calibrated with two standard samples of silver behenate and silicon with beam diameter 0.5 mm for the 10-keV beam (λ = 0.124 nm^{-1}). The electro-optical properties were measured with prepared samples injected in commercially non-rubbed indium-tin-oxide (ITO) cells (mesophase state; thickness 9 μm; active area 0.25 cm^2). With a digital oscilloscope (Tektronix TDS-3012B) connected to a high-power amplifier (Gwinstek) and a function generator (Tektronix AFG 3021), measurements of spontaneous polarization were made with a modified triangular-wave method at a frequency of 50 Hz (see Fig. S1 in the Supporting Information).[62]

Results and discussion

Molecular Structures and Phase Behavior of Synthesized Complexes. As shown in Fig. 2a, single-armed H-bonded bent-core complexes **FIA100** and **SiA100**[61] are composed of proton donor **FIA** (or **SiA**) and acceptor **NBF14** with 1:1 molar ratio; while double-armed H-bonded bent-core complexes **FIIA100** and **IIA100** consist of proton donor **FIIA** (or **IIA**) and acceptor **NBF14** with 1:2 molar ratio. The existence of H-bonded in the mesophases can be proved by temperature-various FTIR spectroscopy (see the Supporting Information). Among these H-bonded bent-core complexes, upon cooling only **SiA100** and **IIA100** processed the smectic CP (SmCP) and smectic C (SmC) phases, respectively. However, the C_{60}-based H-bonded bent-core complexes **FIA100** and **FIIA100** did not display any mesophases in contrast to their C_{60}-based covalent-bonded analogues,[37] because the mesophases were hindered by the stronger aggregation tendency of C_{60}[55] with weaker H-bonds in the H-bonded complexes (i.e., **FIA100** and **FIIA100**). Therefore, **SiA100** was introduced to the H-bonded C_{60}-based bent-core complexes (**FIA100** and **FIIA100**) to extend the mesophasic ranges of the hybrid H-bonded bent-core complexes. As illustrated in Fig. 2b, binary complex **FIA50** was prepared from **FIA**, **SiA** and **NBF14** with 1:1:2 mole ratio and binary complex **FIIA50** was produced by **FIIA**, **SiA** and **NBF14** with 1:2:4 mole ratio. In general, binary complexes **FIAx** and **FIIAx** were denoted as **x** % molar ratio of C_{60}-based bent-core proton donor (i.e., **x** = 4, 24, 50, 76, 90 and 100). For example, since a double-armed proton donor **FIIA** bearing two –COOH functional groups would be H-bonded with two pyridyl moieties of proton acceptor **NBF14** (see Fig. 2b and Table S1 of the Supporting Information). In addition, the relationship for **x** values and weight percents (wt%) of C_{60}-based bent-core complexes are also presented in Table S1 in order to compare with our previous research.[61] As shown in Table 1 and Fig. 3, the broadest mesophasic ranges (upon cooling) of binary complexes **FIAx** and **FIIAx** were both extended from 33.4°C (**SiA100**) to 40.8 (at **x** = 24) and 37.6°C (at **x** = 50), respectively. The POM images of typical broken-fan textures of the SmCP phase for **x** = 24 were shown in Fig. S2 of the Supporting Information.

The single-armed binary complexes **FIAx** displayed lower crystallization temperatures (SmCP-Cr) than their double-armed analogues **FIIAx**, which could be attributed to the colligative property of C_{60}-based complexes. Notably, although most binary complexes possessed monotropic mesophase, only binary complexes **FIA90** and **FIIA90** containing a very high content of C_{60}-based H-bonded bent-core complexes demonstrated narrow mesophasic temperature ranges 11.4 and 10.8°C, respectively (see Fig. 3b). Importantly, higher uptaken loads of C_{60}-based component can be blended into the binary complexes **FIAx** and **FIIAx** (i.e., **x** = 50, 76 and 90 without phase separation) than our previous Au-based covalent-bonded bent-core dopant (phase separation occurred at larger than 20 wt%) in **SiA100**. Therefore, an effective hybrid method for high contents of H-bonded C_{60}-based bent-core complexes was introduced in this study. In addition, by increasing the content of C_{60}-based moiety to moderate values, the polarity of the SmCP phase varied sequentially from anti-ferroelectricity to ferroelectricity in the binary complexes **FIAx** and **FIIAx** (at **x** = 24 ~ 50, see Fig. 3, which was also discussed in the section "**Electro-Optical Properties**").

Table 1 Phase transition temperatures and enthalpies of synthesized compounds and hybrid complexes

Compounds and complexes	Phase transition temperature/°C [enthalpy/J/g][a] heating (top)/ cooling (bottom)
FIA100	**Cr** 89.3[21.0] **Iso** **Iso** 72.3[-18.8] **Cr**
SiA100	**Cr** 97.5[17.1] **SmCP$_A$** 116.4[23.6] **Iso** **Iso** 124.0[-26.5] **SmCP$_A$** 90.6[-13.8] **Cr**
FIIA100	**Cr** 87.0[25.6] **Iso** **Iso** 82.8[-23.6] **Cr**
IIA100	**Cr** 115.5[53.2] **Iso** Iso **127.0**[b] SmC **126.0**[b] Cr
FIA4	**Cr** 97.1[69.2] **Iso** **Iso** 117.5[-30.9] **SmCP$_A$** 87.7[-19.0] **Cr**
FIA24	**Cr** 95.3[36.7] **Iso** **Iso** 120.1[-16.8] **SmCP$_A$** 79.3[-14.4] **Cr**
FIA50	**Cr** 90.5[33.5] **Iso** **Iso** 106.8[-9.1] **SmCP$_F$** 72.8[-15.0] **Cr**
FIA76	**Cr** 87.0[26.9] **Iso** **Iso** 106.1[-0.2] **SmCP$_F$** 73.4[-24.9] **Cr**
FIA90	**Cr** 87.0 [29.5] **Iso** **Iso** 80.4[-1.7] **SmCP$_F$** 69.0[-20.7] **Cr**
FIIA4	**Cr** 98.5[31.8] **Iso** **Iso** 121.8[-17.7] **SmCP$_A$** 88.7[-11.8] **Cr**
FIIA24	**Cr** 98.7[16.8] **SmCP$_A$** 117.0[14.1] **Iso** **Iso** 123.5[-17.0] **SmCP$_A$** 86.8[-17.9] **Cr**
FIIA50	**Cr** 97.5 [36.2] **Iso** **Iso** 115.4[-11.3] **SmCP$_F$** 77.8[-20.1] **Cr**
FIIA76	**Cr** 91.5[33.1] **Iso** **Iso** 100.5[-3.2] **SmCP$_F$** 78.9[-22.8] **Cr**
FIIA90	**Cr** 90.1[31.1] **Iso** **Iso** 88.4[-1.5] **SmCP$_F$** 77.6[-24.0] **Cr**

[a] The phase transitions were measured by DSC at the 2nd heating and 1st cooling scans with a cooling rate of 5°C/min with peak onset., Cr = crystal solid; SmC = smectic C phase; SmCP$_F$ = ferroelectric smectic C phase; SmCP$_A$ = anti-ferroelectric smectic C phase; Iso = isotropic phase.

[b] Mesophases obtained by POM and XRD measurements. (The data of DSC and POM were furnished in Figs. S3 and S4, respectively.)

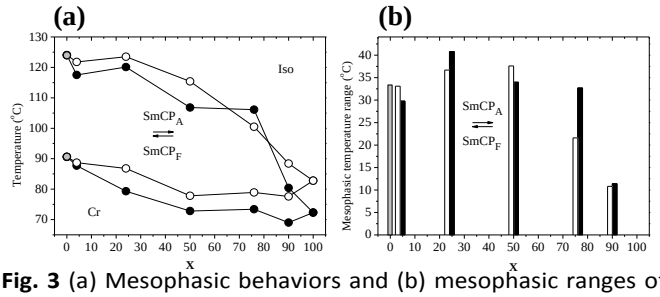

Fig. 3 (a) Mesophasic behaviors and (b) mesophasic ranges of **FIAx** (black), **FIIAx** (white) and **SiA100** (gray).

Molecular structures based on X-ray analysis. In order to decipher the molecular structures of the C_{60}-based bent-core complexes, **FIAx** and **FIIAx** were probed with powder XRD measurements (see Table S2 of the Supporting Information). The C_{60}-based bent-core complexes **FIAx** and **FIIAx** possessed one set of sharp peaks in small angle and broad diffuse scattering signals in wide angle regions indicating a smectic lamellar order of uniformly mixed systems coupled with similar orders of lateral intermolecular distances, respectively (e.g., **x** = 50 shown in Figs. 4a-4c). Sharp peaks indexed as (01) in the small-angle region at the associated d-spacing values of d_1 with 46 ~ 50 Å for hybrid complexes **FIAx** and **FIIAx**, which were shorter than the calculated molecular lengths of **FIA100**, **FIIA100** and **SiA100** (MM+ method, 65 ~ 76 Å) indicating the existence of tilted angles examined in bent-core hybrid complexes (see Table S2). Furthermore, no interdigitated structures are revealed due to the observation of one set ordered diffraction pattern only, and the d-spacing values of **FIAx** and **FIIAx** in Fig. 4c reflected a sequentially descending intensity from (01) to (02) and (03), which indicated simple monolayer organizations instead of C_{60} aggregation-induced bilayer structures with the strongest intensity indexed at (02).[37,63,64] Both hybrid complexes **FIAx** and **FIIAx** possessed similar mesophases of SmCP because of the monolayer structure, rather than a bilayer structure induced by the competitions between Si-based nanosegregations and H-bonds.

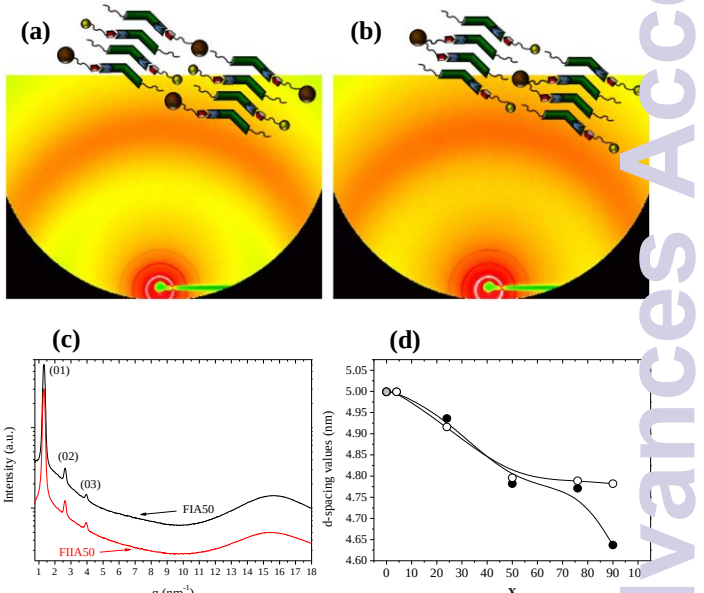

Fig. 4 Proposed molecular orders and XRD patterns of (a) **FIA50** and (b) **FIIA50** as well as (c) both 1-D XRD integrations; (d) the d-spacing values of **FIAx** (black), **FIIAx** (white) and **SiA100** (gray) at T = $T_{Iso-SmCP}$ - 10°C upon cooling.

The d-spacing values of hybrid complexes **FIAx** and **FIIAx** with same **x** values were almost the same, except for **x** = 90 with the largest d-spacing difference possibly due to different measured temperatures (see Fig. 4d and Table 1). Therefore, inferred from the monolayer structures characterized by the XRD measurements of **FIAx** and **FIIAx**, the decreased d-spacing

value of SmCP with increasing C_{60} molar ratio might be mainly attributed to the reduced measured temperature in each hybrid complex, which also suggested that no NP-induced nanosegregations occurred in **FIAx** and **FIIAx**.

Electro-Optical Properties. The electro-optical properties were investigated from the saturated spontaneous polarization (P_s) values obtained via non-rubbed ITO-sandwiched cells to avoid the influence of polyimide layers to ferroelectricity.[65] Under electric fields of modified triangle waveforms, both **FIAx** and **FIIAx** displayed an anti-ferroelectric (AF) to a ferroelectric (FE) polar switching as C_{60} increased:[61] the responsive current signals at the zero-voltage position declined and even vanished as the molar ratio of C_{60}-based moiety with **x** ≧ 50 (see the orange rectangle area marked in Figs. 5a-5b), indicating a ferroelectric polar switching, where the SmCP range was maximized at **x** = 24 (see Table 1). According to the previous research,[65,66] bent-core complexes processed anti-ferroelectric polar switching behavior due to the easy-stacking of bent-shaped molecules with anti-polar order from neighboring layers, but the anti-polar packing could be diminished via NPs aggregated at the smectic layer interfaces. Hence, the switching from anti-ferroelectric to ferroelectric polar order along with C_{60} ratio can be realized from the aggregation of NPs at the interfaces of smectic layers. The trends of P_s values and the saturated P_s values at certain electric fields of hybrid complexes **FIAx** and **FIIAx** are described in Fig. S7. As shown in Fig. 5c, as the C_{60}-based moiety increased, both P_s values of

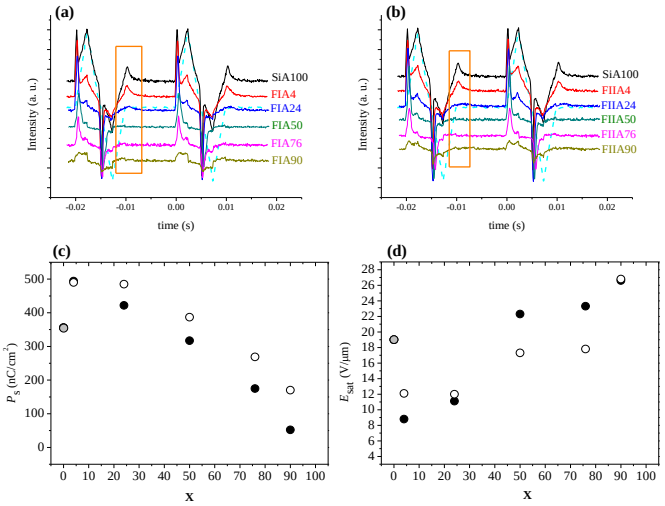

Fig. 5 The saturated P_s values under modified triangular waveforms of (a) **FIAx** and (b) **FIIAx** under SmCP phases; (c) saturated P_s and (d) E_{sat} values of **FIAx** (black), **FIIAx** (white) and **SiA100** (gray) upon cooling. Blue dashed lines indicated applied electric field (33.3 V/μm at 50 Hz), and the orange rectangular was marked as the evidence for AF-FE switching depending on C_{60} molar ratio for **FIA4** and **FIIA24**, respectively. (The detailed switching current responses and POM images to the applied triangular waveform in the mesomorphic phases of **FIA24** ($SmCP_A$) and **FIA76** ($SmCP_F$) are illustrated in Figs. S5 and S6, respectively.)

hybrid complexes **FIAx** and **FIIAx** increased to be saturated at minor C_{60} doped ranges of **x** = 4 ~ 24, which are higher than P_s (356 nC/cm^2) of **SiA100** (at **x** = 0) and reached the largest P_s values of 494 and 490 nC/cm^2 (both at **x** = 4) for **FIAx** and **FIIAx** series, respectively. In addition, the P_s values of **FIAx** and **FIIAx** dropped continuously to become smaller at higher C_{60} doped ranges of **x** = 50 ~ 90. Similarly, in contrast to **FIIAx** with the same **x** values, **FIAx** (at **x** ≧ 24) possessed lower P_s values due to higher C_{60}-based moieties. The minor doping effect of C_{60}-based moiety on promoted P_s values could be attributed to the reinforced separation of induced dipoles by the NP dopants under electric fields.[67] The saturated electric field (E_{sat}) was defined as the electric field at 90% of saturated P_s values (see Fig. S3 of the Supporting Information), and the lowest E_{sat} values of **FIAx** and **FIIAx** series were obtained at 8.8 and 12.0 Vpp/μm for **FIA4** and **FIIA24**, respectively (see Fig. 5d), which were possibly due to the easy driving tendencies of the decreased packing order in the mesophases with minor C_{60}-based contents.[68] By further increasing the ratio of C_{60}-based moiety, the field induced dipole reorientation was restricted by larger viscosities of the mesophases with higher C_{60}-based contents and led to low P_s values and high E_{sat} values.[69] Notably, the saturated P_s value of **SiA100** decayed to half values for **FIAx** and **FIIAx** series at relatively high ratios of C_{60}-based moiety, i.e., **FIAx** at **x** ≧ 76 (i.e., 84 wt%, see Table S1) and **FIIAx** at **x** ≧ 90 (i.e., 92 wt%), which happened in our previous report on Au-based LC composite at 5 wt% of NPs (a relatively low ratio of surface-modified Au NPs).[61] Moreover, in contrast to a low wt% (5 wt%) of surface-modified Au NPs in the previous Au-based LC composite,[61] the AF-FE switching behavior happened at a higher content of surface-modified C_{60} (**x** = 50, i.e., 63 wt% and 56 wt% for **FIAx** and **FIIAx**, respectively) in both hybrid LC complexes. Finally, unlike the phase separation induced in the previous Au-based LC composite containing ~ 20 wt% content of surface-modified Au NPs, much higher contents of surface-modified C_{60} still could be miscible in both **FIAx** and **FIIAx** series at **x** = 90 (i.e., 94 and 92 wt%, respectively), which could be useful to utilize hybrid LC complexes with high contents of surface-modified C_{60}. Therefore, the anti-ferroelectric (AF) to a ferroelectric (FE) polar switching behavior as well as optimized P_s and E_{sat} values could be introduced by adjusting the contents of surface-modified C_{60} in the hybrid LC complexes.

Conclusion

Single- and double-armed C_{60}-based H-bonded bent-core complexes (**FIA100** and **FIIA100**) were mixed with Si-based H-bonded bent-core LC **SiA100** successfully to induce ferroelectric and anti-ferroelectric mesophases, where the hybrid C_{60}-based H-bonded LC complexes are synthesized and reported for the first time. Adjusting various molar ratios of surface-modified C_{60} in the hybrid H-bonded bent-core LC complexes, the transition temperatures and ranges of the SmCP phases could be reduced and extended, respectively. Compared with Au-based LC composites, much higher contents of surface-modified C_{60} could be miscible in both

hybrid LC complexes **FIAx** and **FIIAx** series at **x** = 90 (i.e., 94 and 92 wt%, respectively). The anti-ferroelectric (AF) to a ferroelectric (FE) polar switching behavior occurred in the hybrid LC complexes with moderate molar ratios of C_{60}-based moiety. The electro-optical properties, such as P_s and E_{sat} values, could be manipulated and optimized via the blending ratio of the Si- and C_{60}-based complexes, which could be more easily controlled than the covalent-bonded C_{60}-based LC systems.

Acknowledgements

The financial support of this project is provided by the Ministry of Science and Technology (MOST) in Taiwan through MOST 103-2113-M-009-018-MY3 and 103-2221-E-009-215-MY3. We also thank Drs. Ming-Tao Lee and Hwo-Shuenn Sheu for the assistance of measuring XRD at 13A1 and 01C2 in National Synchrotron Radiation Research Center (NSRRC) in Taiwan.

Notes and references

1 H. W. Kroto, J. R. Heath, S. C. Obrien, R. F. Curl and R. E. Smalley, *Nature*, 1985, **318**, 162-163.
2 M. Arndt, O. Nairz, J. Vos-Andreae, C. Keller, G. van der Zouw and A. Zeilinger, *Nature*, 1999, **401**, 680-682.
3 O. Gunnarsson, *Rev. Mod. Phys.*, 1997, **69**, 575-606.
4 R. C. Haddon, A. F. Hebard, M. J. Rosseinsky, D. W. Murphy, S. J. Duclos, K. B. Lyons, B. Miller, J. M. Rosamilia, R. M. Fleming, A. R. Kortan, S. H. Glarum, A. V. Makhija, A. J. Muller, R. H. Eick, S. M. Zahurak, R. Tycko, G. Dabbagh and F. A. Thiel, *Nature*, 1991, **350**, 320-322.
5 A. F. Hebard, M. J. Rosseinsky, R. C. Haddon, D. W. Murphy, S. H. Glarum, T. T. M. Palstra, A. P. Ramirez and A. R. Kortan, *Nature*, 1991, **350**, 600-601.
6 J. E. Han, O. Gunnarsson and V. H. Crespi, *Phys. Rev. Lett.*, 2003, **90**, 167006.
7 W. J. Blau, H. J. Byrne, D. J. Cardin, T. J. Dennis, J. P. Hare, H. W. Kroto, R. Taylor and D. R. M. Walton, *Phys. Rev. Lett.*, 1991, **67**, 1423-1425.
8 R. Mitsumoto, T. Araki, E. Ito, Y. Ouchi, K. Seki, K. Kikuchi, Y. Achiba, H. Kurosaki, T. Sonoda, H. Kobayashi, O. V. Boltalina, V. K. Pavlovich, L. N. Sidorov, Y. Hattori, N. Liu, S. Yajima, S. Kawasaki, F. Okino and H. Touhara, *J. Phys. Chem. A*, 1998, **102**, 552-560.
9 Z. Xiao, D. He, C. Zuo, L. Gan and L. Ding, *RSC Adv.*, 2014, **4**, 24029-24031.
10 G. V. Andrievsky, V. K. Klochkov, A. B. Bordyuh and G. I. Dovbeshko, *Chem. Phys. Lett.*, 2002, **364**, 8-17.
11 G. Andrievsky, V. Klochkov and L. Derevyanchenko, *Fuller. Nanotub. Carbon Nanostruct.*, 2005, **13**, 363-376.
12 G. V. Andrievsky, V. I. Bruskov, A. A. Tykhomyrov and S. V. Gudkov, *Free Radic. Biol. Med.*, 2009, **47**, 786-793.
13 Y. F. Zhao, Y. H. Kim, A. C. Dillon, M. J. Heben and S. B. Zhang, *Phys. Rev. Lett.*, 2005, **94**, 155504.
14 S. H. Wang and S. A. Jansen, *J. Phys. Chem.*, 1995, **99**, 8556-8561.
15 R. Eigler, F. W. Heinemann and A. Hirsch, *Chem. Commun.*, 2014, **50**, 2021-2023.
16 N. C. Maliszewskyj, P. A. Heiney, D. R. Jones, R. M. Strongin, M. A. Cichy and A. B. Smith, *Langmuir*, 1993, **9**, 1439-1441.
17 M. Prato, T. Suzuki, H. Foroudian, Q. Li, K. Khemani, F. Wudl, J. Leonetti, R. D. Little, T. White, B. Rickborn, S. Yamago and E. Nakamura, *J. Am. Chem. Soc.*, 1993, **115**, 1594-1595.
18 I. Fernández, M. Solà and F. M. Bickelhaupt, *Chem.-Eur. J.*, 2013, **19**, 7416-7422.
19 M. S. Markoulides, G. I. Ioannou, M. J. Manos and N. Chronakis, *RSC Adv.*, 2013, **3**, 4750-4756.
20 D. M. Guldi, H. Hungerbuhler, E. Janata and K. D. Asmus, *J. Phys. Chem.*, 1993, **97**, 11258-11264.
21 V. Bandi, M. E. El-Khouly, K. Ohkubo, V. N. Nesterov, M. E. Zandler, S. Fukuzumi and F. D'Souza, *Chem.-Eur. J.*, 2013, **19**, 7221-7230.
22 A. Kremer, E. Bietlot, A. Zanelli, J. M. Malicka, N. Armaroli and D. Bonifazi, *Chem.-Eur. J.*, 2015, **21**, 1108-1117.
23 B. Elliott, K. Yang, A. M. Rao, H. D. Arman, W. T. Pennington and L. Echegoyen, *Chem. Commun.*, 2007, DOI: 10.1039/b700320j, 2083-2085.
24 A. Rodriguez-Fortea, A. L. Balch and J. M. Poblet, *Chem. Soc. Rev.*, 2011, **40**, 3551-3563.
25 V. Campisciano, V. La Parola, L. F. Liotta, F. Giacalone and M. Gruttadauria, *Chem.-Eur. J.*, 2015, **21**, 3327-3334.
26 L. Chao, L. Lu, H. Yang, Y. Zhu, Y. Li, Q. Wang, X. Yu, S. Jiang and Y.-H. Chen, *PLoS One*, 2013, **8**, e66156.
27 L. Wang, X. Zhu, X. Tang, C. Wu, Z. Zhou, C. Sun, S.-L. Deng, H. Ai and J. Gao, *Chem. Commun.*, 2015, **51**, 4390-4393.
28 S.-H. Chan, C.-S. Lai, H.-L. Chen, C. Ting and C.-P. Chen, *Macromolecules*, 2011, **44**, 8886-8891.
29 M.-E. Ragoussi and T. Torres, *Chem. Commun.*, 2015, **51**, 3957-3972.
30 R. J. Bushby, I. W. Hamley, Q. Y. Liu, O. R. Lozman and J. E. Lydon, *J. Mater. Chem.*, 2005, **15**, 4429-4434.
31 T. Chuard and R. Deschenaux, *J. Mater. Chem.*, 2002, **12**, 1944-1951.
32 W. L. Ma, C. Y. Yang, X. Gong, K. Lee and A. J. Heeger, *Adv. Funct. Mater.*, 2005, **15**, 1617-1622.
33 X. N. Yang, J. Loos, S. C. Veenstra, W. J. H. Verhees, M. M. Wienk, J. M. Kroon, M. A. J. Michels and R. A. J. Janssen, *Nano Lett.*, 2005, **5**, 579-583.
34 T. Wang, X. Liao, J. Wang, C. Wang, M.-Y. Chan and V. W.-W. Yam, *Chem. Commun.*, 2013, **49**, 9923-9925.
35 J. Kelber, M.-F. Achard, B. Garreau-de Bonneval and H. Bock, *Chem.-Eur. J.*, 2011, **17**, 8145-8155.
36 X. Chen, L. Chen and Y. Chen, *RSC Adv.*, 2014, **4**, 3627-3632.
37 J. Vergara, J. Barbera, J. Luis Serrano, M. Blanca Ros, N. Sebastian, R. de la Fuente, D. O. Lopez, G. Fernandez, L. Sanchez and N. Martin, *Angew. Chem.-Int. Edit.*, 2011, **50**, 12523-12528.
38 T. N. Y. Hoang, D. Pociecha, M. Salamonczyk, E. Gorecka and R. Deschenaux, *Soft Matter*, 2011, **7**, 4948-4953.
39 H. Mamlouk, B. Heinrich, C. Bourgogne, B. Donnio, D. Guillon and D. Felder-Flesch, *J. Mater. Chem.*, 2007, **17**, 2199-2205.
40 S. Campidelli, T. Brandmueller, A. Hirsch, I. M. Saez, J. W. Goodby and R. Deschenaux, *Chem. Commun.*, 2006, DOI: 10.1039/b610350b, 4282-4284.
41 S. Campidelli, P. Bourgun, B. Guintchin, J. Furrer, H. Stoeckli-Evans, I. M. Saez, J. W. Goodby and R. Deschenaux, *J. Am. Chem. Soc.*, 2010, **132**, 3574-3581.
42 E. Allard, F. Oswald, B. Donnio, D. Guillon, J. L. Delgado, F. Langa and R. Deschenaux, *Org. Lett.*, 2005, **7**, 383-386.
43 J. Lenoble, S. Campidelli, N. Maringa, B. Donnio, D. Guillon, [illegible]. Yevlampieva and R. Deschenaux, *J. Am. Chem. Soc.*, 2007, **129**, 9941-9952.

44 C.-Z. Li, Y. Matsuo and E. Nakamura, *J. Am. Chem. Soc.*, 2009, **131**, 17058-17059.
45 T. T. Nguyen, S. Albert, T. L. A. Nguyen and R. Deschenaux, *RSC Adv.*, 2015, **5**, 27224-27228.
46 T. Kato, T. Yasuda, Y. Kamikawa and M. Yoshio, *Chem. Commun.*, 2009, 729-739.
47 M. Lehmann and M. Hügel, *Angew. Chem.-Int. Edit.*, 2015, **54**, 4110-4114.
48 X. Zhang, C. H. Hsu, X. Ren, Y. Gu, B. Song, H. J. Sun, S. Yang, E. Chen, Y. Tu and X. Li, *Angew. Chem.-Int. Edit.*, 2015, **54**, 114-117.
49 M. Sawamura, K. Kawai, Y. Matsuo, K. Kanie, T. Kato and E. Nakamura, *Nature*, 2002, **419**, 702-705.
50 Y. Matsuo, A. Muramatsu, Y. Kamikawa, T. Kato and E. Nakamura, *J. Am. Chem. Soc.*, 2006, **128**, 9586-9587.
51 H. N. Ghosh, K. Adamczyk, S. Verma, J. Dreyer and E. T. J. Nibbering, *Chem.-Eur. J.*, 2012, **18**, 4930-4937.
52 (a) V. Vagenende, T.-J. Ching, R.-J. Chua, N. Thirumoorthi and P. Gagnon, *ACS Appl. Mater. Interfaces*, 2013, **5**, 4472-4478. (b) M. Wei, M. Zhan, D. Yu, H. Xie, M. He, K. Yang and Y. Wang, *ACS Appl. Mater. Interfaces*, 2015, **7**, 2585-2596.
53 (a) D. Felder-Flesch, L. Rupnicki, C. Bourgogne, B. Donnio and D. Guillon, *Journal of Materials Chemistry*, 2006, **16**, 304-309. (b) W.-S. Li, Y. Yamamoto, T. Fukushima, A. Saeki, S. Seki, S. Tagawa, H. Masunaga, S. Sasaki, M. Takata and T. Aida, *Journal of the American Chemical Society*, 2008, **130**, 8886-8887.
54 (a) P. H. J. Kouwer and G. H. Mehl, *Journal of Materials Chemistry*, 2009, **19**, 1564-1575. (b) R. Deschenaux, B. Donnio and D. Guillon, *New Journal of Chemistry*, 2007, **31**, 1064-1073. (c) S. D. Peroukidis, A. G. Vanakaras and D. J. Photinos, *The Journal of Physical Chemistry B*, 2008, **112**, 12761-12767. (d) J. Vergara, J. Barberá, J. L. Serrano, M. B. Ros, N. Sebastián, R. de la Fuente, D. O. López, G. Fernández, L. Sánchez and N. Martín, *Angewandte Chemie*, 2011, **123**, 12731-12736.
55 (a) T. Michinobu, T. Nakanishi, J. P. Hill, M. Funahashi and K. Ariga, *J. Am. Chem. Soc.*, 2006, **128**, 10384-10385. (b) L.-Y. Wang, I. H. Chiang, P.-J. Yang, W.-S. Li, I. T. Chao and H.-C. Lin, *J. Phys. Chem. B*, 2009, **113**, 14648-14660.
56 S. Kimura, S. Nishiyama, Y. Ouchi, H. Takezoe and A. Fukuda, *Jpn. J. Appl. Phys.*, 1987, **26**, L255-L257.
57 H. Okada, T. Sakurai, T. Katoh, M. Watanabe, H. Onnagawa, N. Nakatani and K. Miyashita, *Jpn. J. Appl. Phys.*, 1993, **32**, 4339-4343.
58 H. Okada, K. Kurabayashi, Y. Kidoh, H. Onnagawa and K. Miyashita, *Jpn. J. Appl. Phys.*, 1994, **33**, 4666-4672.
59 S. Essid, M. Manai, A. Gharbi, J. P. Marcerou and J. C. Rouillon, *Liq. Cryst.*, 2005, **32**, 307-313.
60 N. Podoliak, O. Buchnev, M. Herrington, E. Mavrona, M. Kaczmarek, A. G. Kanaras, E. Stratakis, J.-F. Blach, J.-F. Henninot and M. Warenghem, *RSC Adv.*, 2014, **4**, 46068-46074.
61 W.-H. Chen, Y.-T. Chang, J.-J. Lee, W.-T. Chuang and H.-C. Lin, *Chem.-Eur. J.*, 2011, **17**, 13182-13187.
62 K. Miyasato, S. Abe, H. Takezoe, A. Fukuda and E. Kuze, *Jpn. J. Appl. Phys.*, 1983, **22**, L661-L663.
63 S. Campidelli, R. Deschenaux, J. F. Eckert, D. Guillon and J. F. Nierengarten, *Chem. Commun.*, 2002, DOI: 10.1039/b111595b, 656-657.
64 C. Keith, R. A. Reddy, A. Hauser, U. Baumeister and C. Tschierske, *J. Am. Chem. Soc.*, 2006, **128**, 3051-3066.
65 C. Keith, R. A. Reddy, M. Prehm, U. Baumeister, H. Kresse, J. L. Chao, H. Hahn, H. Lang and C. Tschierske, *Chem.-Eur. J.*, 2007, **13**, 2556-2577.
66 C. L. Folcia, J. Ortega, J. Etxebarria, S. Rodriguez-Conde, G. Sanz-Enguita, K. Geese, C. Tschierske, V. Ponsinet, P. Barois, R. Pindak, L. Pan, Z. Q. Liu, B. K. McCoy and C. C. Huang, *Soft Matter*, 2014, **10**, 196-205.
67 D. P. Singh, S. K. Gupta and R. Manohar, *Adv. Condens. Matter Phys.*, 2013, DOI: 10.1155/2013/250301, 250301.
68 T. Zhang, C. Zhong and J. Xu, *Jpn. J. Appl. Phys.*, 2009, **48**, 055002.
69 O. Francescangeli, V. Stanic, S. I. Torgova, A. Strigazzi, N. Scaramuzza, C. Ferrero, I. P. Dolbnya, T. M. Weiss, R. Berardi, L. Muccioli, S. Orlandi and C. Zannoni, *Adv. Funct. Mater.*, 2009, **19**, 2592-2600.